Helium Transport, Fate and Management in Nanostructured Ferritic Alloys: In Situ Helium Implanter Studies – G. R. Odette, P. Miao, T. Yamamoto (University of California Santa Barbara, Santa Barbara), D. J. Edwards, R. J. Kurtz (Pacific Northwest National Laboratory) and H. Tanigawa (Japan Atomic Energy Agency)

OBJECTIVE

Objective of the study to understand transport and fate of transmutation helium using thin Ni-bearing implanter layers to inject high-energy a-particles into an adjacent sample simultaneously undergoing neutron induced displacement damage. We summarize here the results of microstructural studies on a 14Cr-NFA, MA957, following HFIR irradiations at 500°C to 9 dpa and 380 appm, with a focus on TEM characterization of cavities formation and the association of these cavities with NF and other interfaces.

SUMMARY

High helium levels produced in fusion neutron spectra may lead to severe increases in the brittle fast fracture temperature, enhanced void swelling and degradation of creep rupture properties at lower, intermediate and higher irradiation temperatures, respectively. Thus it is important to develop structural alloys with stable microstructures that can manage helium based on understanding of its transport, fate and consequences. We report on the initial results of a study of helium f in a nanostructured ferritic alloy (NFA), MA957, that is dispersion strengthened by an ultra-high density of nm-scale Y-Ti-O nanofeatures (NF). An in situ helium implanter technique uniformly deposited ≈ 380 appm helium to ≈ 6 µm in MA957 irradiated in the High Flux Isotope Reactor (HFIR) ≈ to 9 dpa at 500°C. Through focus transmission electron microscopy (TEM) showed that helium is in extremely fine bubbles that often appear to coincide with bright field features taken as NF.

PROGRESS AND STATUS

Introduction

Predicting and mitigating the effects of a combination of large levels of transmutant helium and displacement damage (dpa) produced by high energy neutrons on the dimensional stability and mechanical properties of structural materials is one of the key challenges to developing of fusion energy. Fundamental questions about helium-dpa synergisms include: a) what are the basic interacting mechanisms controlling helium and defect transport, fate and consequences, and how are they influenced by the microstructural and irradiation (dpa rate, He/dpa ratio, temperature and applied stress) variables; and, b) how can the detrimental effects of high He-dpa synergisms be mitigated and managed by proper microstructural design? We have proposed that NFA containing an ultra-high density of NF that pin dislocations, resulting in remarkably high creep strength, could mitigate radiation damage by trapping helium in fine bubbles, while permitting operation at temperatures above the displacement damage accumulation regime [1].

We have shown that in-situ He implantation in mixed spectrum fission reactor irradiations provides a very attractive approach to assessing the effects of helium-dpa synergisms [2-7]. The basic idea is to use thin Ni (or B or Li)-bearing implanter layers to inject high-energy a-particles into an adjacent sample simultaneously undergoing neutron induced displacement damage. In this case, irradiations in the HFIR uniformly implanted 4.8 MeV a-particles (helium) to a depth of ≈ 5 to 8 mm at controlled helium/dpa ratios from ≈ 5 to 40 appm/dpa. The helium -implanted region is suitable for extensive microstructural characterization by TEM (and, potentially, a variety of other techniques) and is sufficiently thick to permit low load microhardness or nanohardness measurements. We summarize here the results of microstructural studies on a 14Cr NFA, MA957, following HFIR irradiations at 500°C to 9 dpa and 380 appm. These results focus on TEM characterization of the transport and fate of helium in forming cavities (helium bubbles), and the association of these cavities with NF and other interfaces. These observations

are briefly compared to the corresponding results for an 8Cr normalized and tempered martensitic steel (TMS), F82H, reported elsewhere [7].

Experimental Procedures

The Fe-14Cr, 0.9Ti, 0.3Mo and 0.5Y_2O_3 (wt.%) INCO MA957, examined in this study, was supplied by A. Alamo (CEA) in the form of a 9 mm thick, 65 mm outer diameter thick-walled tubing. The tube was fabricated by center drilling an as-extruded bar followed by hot extrusion to form the tube. Further details of the processing history of the French MA957 tube are not available. However, the micro and nanostructures of the French MA957 broadly resemble that found in a US heat of MA957 in the 1150°C as-extruded condition. Small angle neutron scattering (SANS) measurements show the French MA957 contains ≈ $7x10^{23}/m^3$ NF with an average diameter of ≈ 2.6 nm and volume fraction of 0.7% [8].

Three mm diameter, 0.2 mm thick TEM discs were irradiated in the HFIR JP26 experiment at 300, 400 and 500°C to produce a range of dpa and He/dpa for a large matrix of alloys, including the French MA957 studied here. A thin NiAl intermetallic layer was electron beam co-deposited at UCSB on discs that were paired with adjacent uncoated discs. Target coating thicknesses of 1, 2 and 4 μm produced nominal He/dpa ratios of 5, 20, and 40 at 9 dpa.

An electron transparent TEM specimen was prepared by focused ion beam micromachining (FIBed). The initial FIBed specimen contained substantial amounts of surface contamination, including features that could be easily confused with NF or bubbles [5]. Thus the specimen was re-FIBed and subsequently plasma cleaned prior to re-examination at the Pacific Northwest National Laboratory (PNNL) on a 200 keV JEOL 2010F TEM in transmission with digitally recorded images. A flash polishing techniques was also developed involving ≈ 5 second electro-polishing in 2% perchloric/2-butoxyethanol solution to further clean-up the specimen surfaces; however, flash polishing was not found to be necessary in this study. The TEM characterization focused on the NF and helium bubbles. The NF were imaged under both bright field and weak beam dark field conditions. The NF observed in TEM were found to be broadly comparable to those found in the SANS studies as well as with other TEM studies at UCSB [8]. The cavities were primarily characterized by the through-focus sequence technique. They appear as white regions surrounded by a dark ring in the under-focused condition (-512 to -1024 nm), as dark regions surrounded by white rings in the over-focused condition (+512 to +1024 nm); the cavities are largely invisible in the focused condition. Local foil thicknesses were measured by convergent beam electron diffraction (CBED).

Given the very small size of the cavities, special efforts applied to the image analysis of the micrographs. The features observed in the three sets of images processed by Photoshop for the through focus sequence were individually identified by overlay comparisons. Cavities were identified as those features that clearly showed a bright-dark contrast in the under-over focus conditions. The NF were identified as those features appearing under in-focus conditions. Cavities are found in both the matrix and in probable association with the NF and larger precipitates. Of course, it is not possible to ensure the absence of some artifacts in these observations, particularly since the cavities are so small. Thus some features that are not cavities may be counted as such, while other cavities may remain invisible. The results unambiguously show the absence of larger cavities, such as those observed in TMS (see below) [7], and this conclusion is further supported by the fact that cavities are generally not observed in the un-implanted regions of the irradiated French MA957. Thus the results described below represent a best estimates of the cavity population in the helium implanted French MA957.

Experimental Results

Figure 1 shows a typical through-focus sequence image for the implanted region at -1024 nm underfocus (a), +512 overfocus (b) and in-focus (c) imaging conditions. The imaging sequence showed a high degree of association between over-focused, darkly imaging features and under-focused, brightly imaging features (again note, the features that did not image in both cases were not counted as cavities). There is

also a high, but slightly smaller, association between the cavities and particles that show contrast for the in-focus condition, which are assumed to be NF. The micrographs also show that cavity-NF combinations appear to be fairly frequently associated with dislocation line segments. Figure 1d illustrates the general absence of cavities in the un-implanted region. Figure 2 shows the cavity size distribution in the helium implanted MA957 compared to that observed in TMS F82H-mod.3 [7]. The size distribution is much narrower in the MA957, with a maximum cavity diameter of less than 2.5 nm and an average diameter of 1.3 nm. In contrast, the largest cavity diameters exceed 10 nm in F82H, with an average value of 2.8 nm. The corresponding number densities are $4.3 \times 10^{23}/m^3$ and $5 \times 10^{22}/m^3$ for MA957 and F82H, respectively. Figure 3 shows another -1024 under-focused image of an implanted region containing larger particles and a boundary. Examples of the decoration of particles with associated cavities are shown in the inserts. The boundary appears to be relatively cavity free, and there does not seem to be a large nearby NF-cavity denuded zone. Figure 4 shows blow up views of through focus sequence images of cavities attached to larger particles.

Discussion

While we have referred to cavities in the previous discussion, it seems likely that these features are actually near-equilibrium helium bubbles with a gas pressure $P_g \approx 3Z(P_g)mkT/4\pi r_b^3 \approx 2g/r_b$ [10], where g is the surface energy, r_b is the bubble radius, m is the number of helium atoms in the bubble and $Z(P_g)$ is the compressibility factor (> 1) for high pressure helium [10]. Assuming equal partitioning of all the 380 appm helium to 4.3×10^{23} bubbles/m^3 (≈ 70 helium atoms/bubble) and g =2 J/m^2 gives $r_b \approx 1.3$ nm at 500°C, in remarkable agreement with the measured average cavity size. Thus we conclude that helium in the implanted MA957 is primarily stored in near-equilibrium bubbles at a capillary pressure of $2g/r_b \approx$ 2670 MPa. A higher helium content of 2000 appm helium partitioned to the same number of bubbles (≈ 370 helium atoms/bubble) increases r_b to 2.2 nm. Note, once established helium bubbles act as very deep traps for helium. Thus the helium stored in matrix bubbles is prevented from reaching and thereby embrittling grain boundaries.

Such microstructures are also highly resistant to void swelling. Voids are cavities with P_g < to << $2g/r_b$ that unstably grow by accumulating an excess flux of vacancies over self-interstitial atoms (SIA) flowing to them, due to a bias of dislocation sinks for the SIA [1,11-13]. For a specified sink microstructure and irradiation condition, cavities grow as stable bubbles up to a critical helium content, m*, where they convert to unstably growing voids, leading to bimodal cavity size distributions [10-13]. Thus the incubation dose, dpa_i, prior to the onset of rapid void swelling is governed by the requirement that a significant population of bubbles reach the $m \geq m^*$ condition. A corollary is that the incubation dose, dpa_i, decreases with the number of bubbles.

However, helium bubbles also act as neutral sinks for annihilating and equal number of vacancies and SIA. The corresponding sink strength is $Z_b \approx 4\pi r_b N_b$, or $\approx 7 \times 10^{15}/m^2$ for $4.3 \times 10^{23}/m^3$, 1.3 nm bubbles, is much higher that typical of other sinks, including SIA biased dislocations (typically $Z_d < 1 \times 10^{15}/m^2$). Such high neutral sink strength results in a low radiation induced vacancy flow excess, $D_vX_v - D_iX_i$, where D is the diffusion coefficient and X the atomic fraction of vacancies (v) and SIA (i), respectively. The effective vacancy super-saturation is defined as $f = [D_vX_v - D_iX_i + D_{sd}]/D_{sd}$, where D_{sd} is the self-diffusion coefficient. If f is low (≈ 1), which is the case for large Z_d, then m*, which is proportional to $\approx 1/[1 - f]^2$, is so large that voids do not nucleate [1,10-13]; and even if they did vacancies would accumulate at a slow rate due to the dominance of neutral bubble sink vacancy-SIA recombination centers [1,10-13]. A corollary is that the flow and accumulation of SIA would also be reduced, presumably resulting in lower rates of loop evolution and other related processes such as irradiation creep, enhanced diffusion and induced solute segregation. Further discussion of the elements of radiation damage resistance can be found in Reference [1].

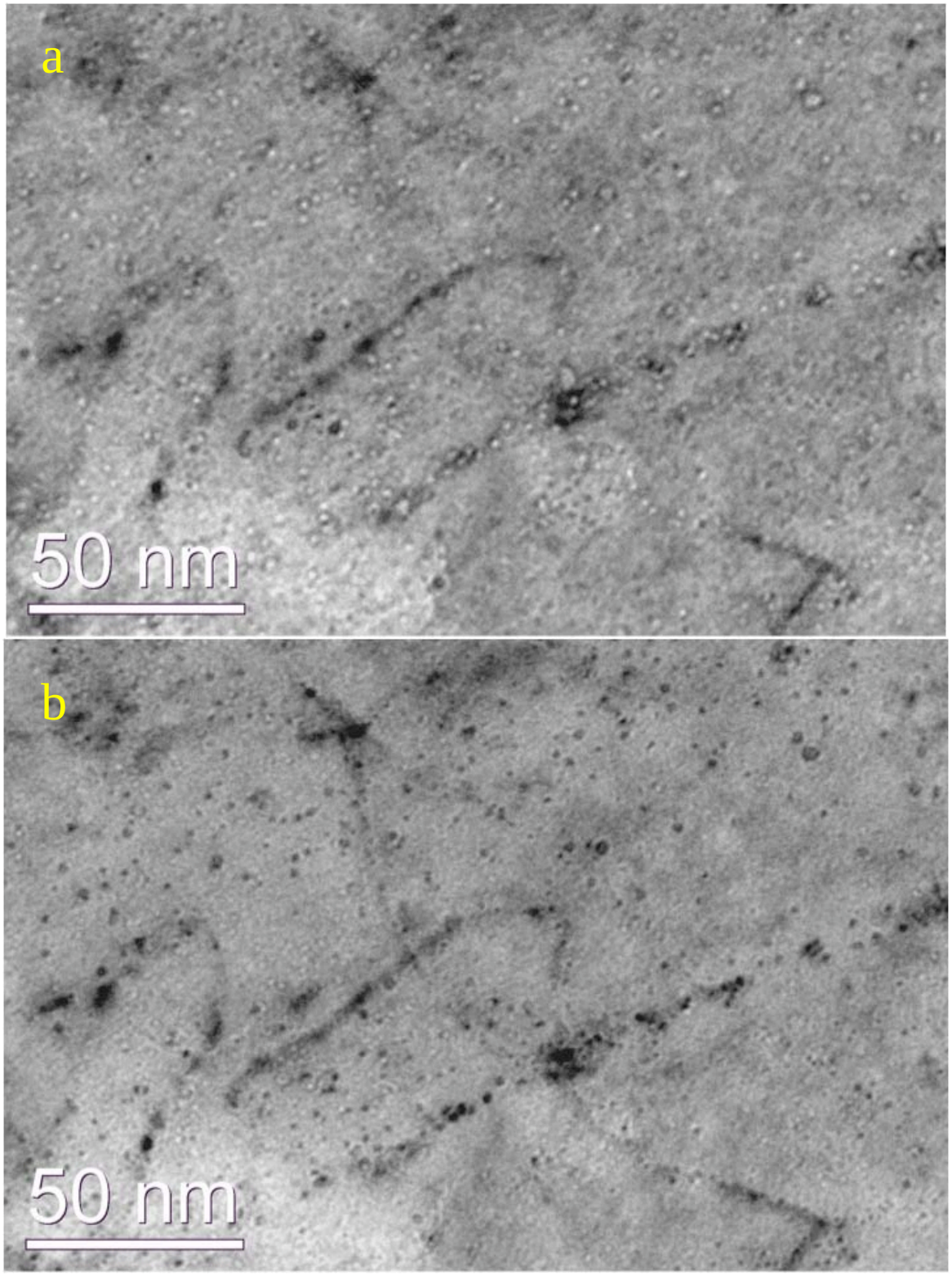

Figure 1 TEM bright field images: a) -1048 under-focus; b) +524 over-focus.

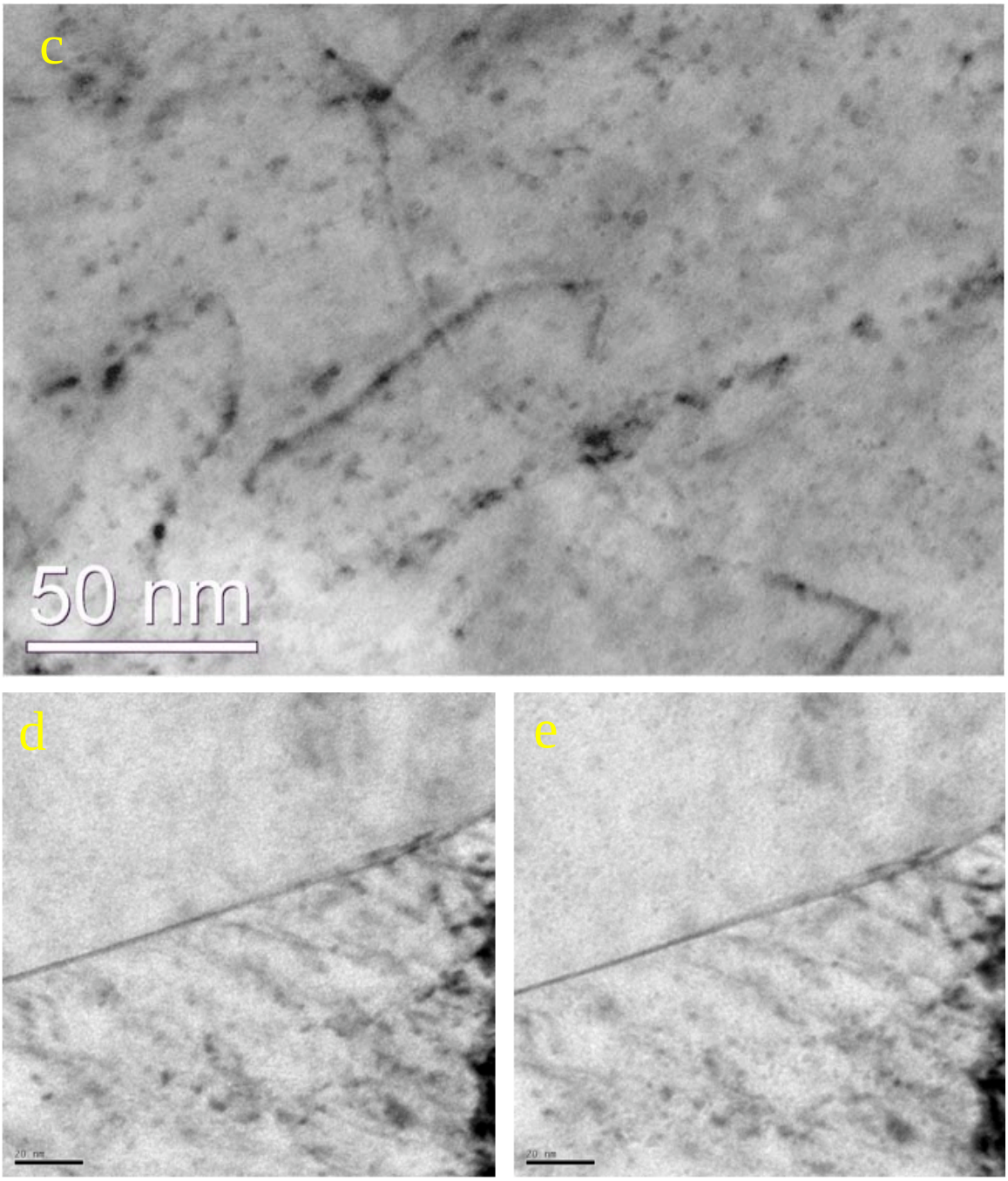

Figure 1 (cont.) c) in-focus BF images of particles assumed to be NF; d) ±524 nm over/under-focus images of on un-implanted region

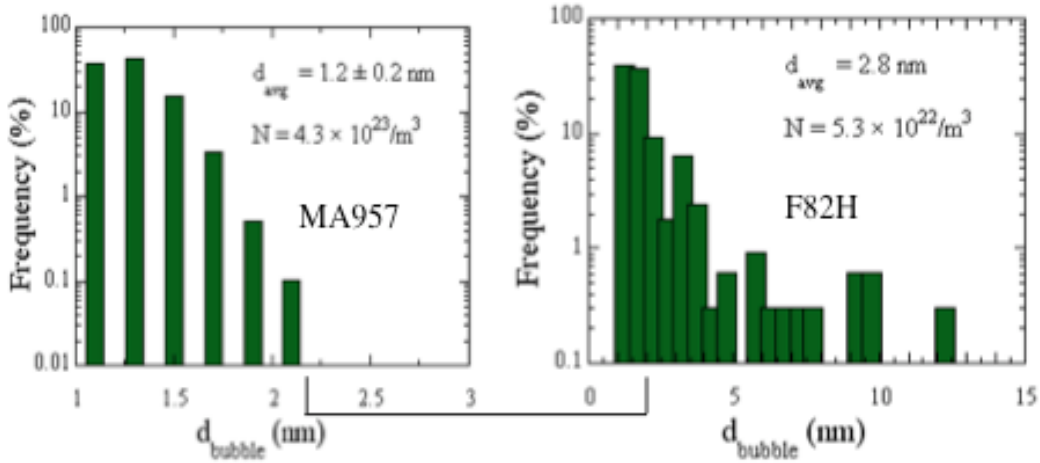

Figure 2 The cavity size distribution in helium imp[lanted MA957 compared to that observed in TMS F82H.

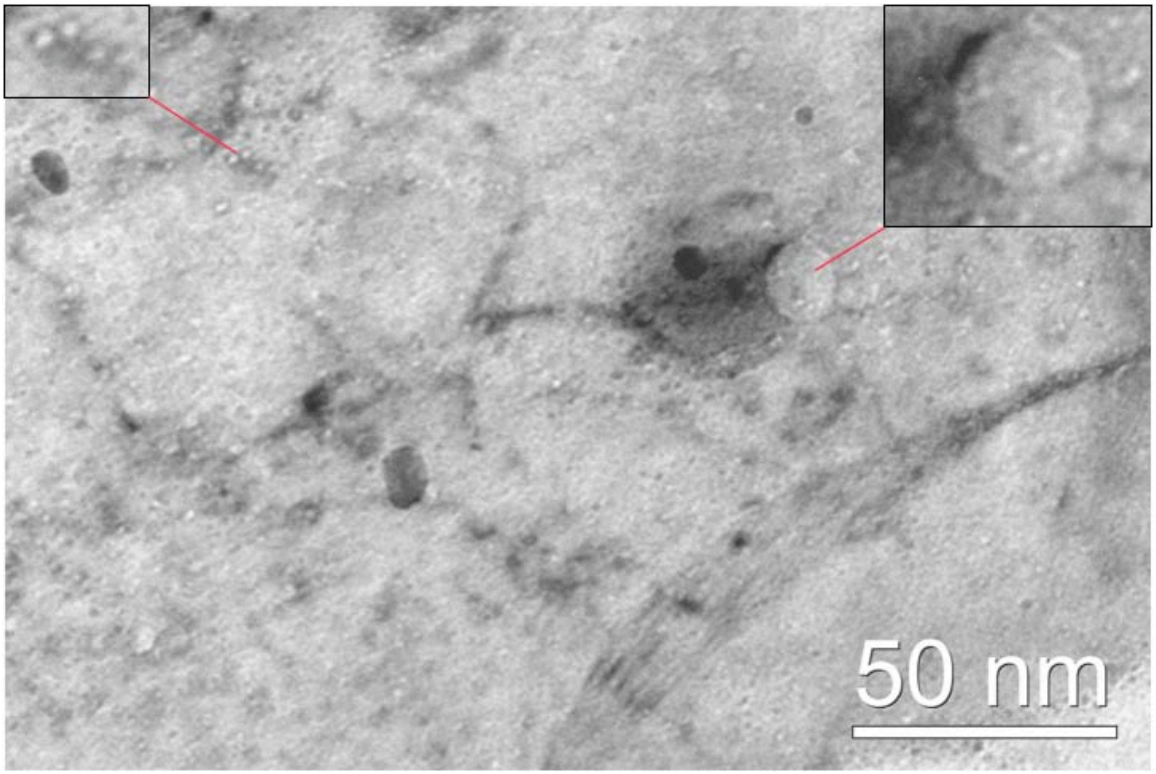

Figure 3 TEM bright field -1048 under-focus images showing matrix particles and a boundary. The insert blow-ups show cavities on larger particles.

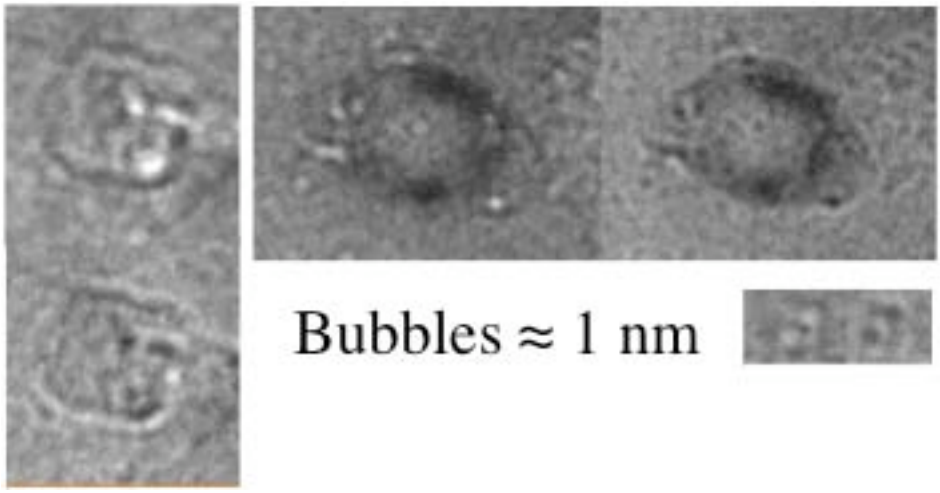

Figure 4. Through focus series images showing cavities on larger particles.

Concluding Remarks

An in-situ injection technique was used to study the transport and fate of helium in NFA MA957 irradiated in HFIR to 9 dpa at 500°C at a nominal helium/dpa ratio of 40 appm/dpa. A very high density of nm-scale bubbles was observed. The bubbles were preferentially associated with dislocations, and NF and precipitate interfaces. However, grain boundaries appeared to be relatively bubble free. These initial results barely scratch the surface of what can be learned about the transport, fate and consequences of helium using the in situ injection technique. Thus in addition to further characterization studies of the alloys and irradiation conditions described in this and previous publications, a major future effort will be directed at characterizing the large matrix of other alloys and irradiation conditions from the JP26 and JP27 experiments, that contained a total of ≈ 360 He injected TEM discs.

Future Research

Post irradiation examination of the large matrix of in situ implanted alloys is continuing as part of UCSB collaborations with PNNL, LANL and ORNL. Notably, specimens are now available fro the JP27 experiment with much higher levels of He up to 1400 appm at 22 dpa at 500°C

Acknowledgements

This research was supported by the U. S. Department of Energy, Office of Fusion Energy Sciences, under contracts DE-FG03-94ER54275 (UCSB) and DE-AC06-76RLO1830 (PNNL). The authors also acknowledge the significant contributions of R. Stoller and D. Hoelzer as well as their Oak Ridge National Laboratory colleagues in contribution a large amount of time and effort to the HFIR irradiations and providing the specimens for examination.

References

[1] G. R. Odette, M. J. Alinger, B. D. Wirth, *Annual Review of Materials Research* 38, 471 (2008).
[2] G.R. Odette, *J. Nucl. Mat.* 141 (1986) 101
[3] L.K. Mansur and W.A. Coghlan, Effects of Irradiation on Materials-14, ASTM STP 1046, 315 (1989).
[4] T. Yamamoto, G. R. Odette, L. R. Greenwood, *Fusion Materials Semiannual Report 1/1 to 6/30/2005* DOE/ER-313/38, 95 (2005).

[5] T. Yamamoto, G. R. Odette, P. Miao, D. T. Hoelzer, J. Bentley, N. Hashimoto, H. Tanigawa, R. J. Kurtz, *J. Nucl. Mater.* 367-370, 399 (2007).
[6] R.J. Kurtz, G.R. Odette, T. Yamamoto, D.S. Gelles, P. Miao, B.M. Oliver, *J. Nucl. Mater.* 367-370, 417 (2007).
[7] T. Yamamoto, G.R. Odette, P. Miao, D.J. Edwards, R.J. Kurtz, *J Nuc Mater*. 386-388, 338 (2009).
[8] M. J. Alinger, G. R. Odette, and D. T. Hoelzer, Acta Mater. 57, 392 (2009).
[9] P. Miao, G. R. Odette, T. Yamamoto, M. J. Alinger and D. Klingensmith, *J Nuc Mater 377*, 59 (2008)
[10] R. E. Stoller and G. R. Odette, *J. Nucl. Mater.* 131, 118 (1985).
[11] G.R. Odette, "On Mechanisms Controlling Swelling in Ferritic Alloy and Martensitic Alloys", *J. Nucl. Mat*. 154, 921 (1988).
[12] G.R. Odette, P.J. Mazaisz and J.A. Spitznagel, *J. Nucl. Mat*. 103, 1239 (1981).
[13] G.R. Odette, "Modeling Microstructural Evolution in Fusion Reactor Environment", *J. Nucl. Mat*. 133, 127 (1985).